SIMULATION OF THE CASIMIR EFFECT FOR VARIOUS GEOMETRIES

A THESIS SUBMITTED TO
THE GRADUATE SCHOOL OF NATURAL AND APPLIED SCIENCES
OF
THE MIDDLE EAST TECHNICAL UNIVERSITY

BY

EMRE TAŞCI

IN PARTIAL FULFILLMENT OF THE REQUIREMENTS FOR THE DEGREE OF

MASTER OF SCIENCE

IN

THE DEPARTMENT OF PHYSICS

JULY 2002

Approval of the Graduate School of Natural and Applied Sciences

Prof. Dr. Tayfur Öztürk
Director

I certify that this thesis satisfies all the requirements as a thesis for the degree of Master of Science.

Prof. Dr. Sinan Bilikmen
Head of Department

This is to certify that we have read this thesis and that in our opinion it is fully adequate, in scope and quality, as a thesis for the degree of Master of Science.

Prof. Dr. Şakir Erkoç
Supervisor

Examining Committee Members

Prof. Dr. Şakir Erkoç _____

Prof. Dr. Lemi Türker _____

Prof. Dr. Cemal Yalabık _____

Prof. Dr. Demet Gülen _____

Prof. Dr. O. Amdulla Mekhrabov _____

ABSTRACT

SIMULATION OF THE CASIMIR EFFECT FOR VARIOUS GEOMETRIES

Taşcı, Emre

M.S., Department of Physics

Supervisor: Prof. Dr. Şakir Erkoç

July 2002, 54 pages

This thesis aims to propose an algorithm in order to calculate the Casimir effect and after, by means of this algorithm, to expand the applications of the effect for various geometries that are difficult to construct in experimental conditions. Theoretical, as well as experimental results have been given and revised in order to check the reliability of the algorithm in question.

Keywords: Casimir Effect, Vacuum Energy, Atomic Interaction Simulation

ÖZ

CASIMIR ETKİSİNİN FARKLI GEOMETRİLERDE SİMÜLASYONU

Taşcı, Emre

Yüksek Lisans, Fizik Bölümü

Tez Yöneticisi: Prof. Dr. Şakir Erkoç

Temmuz 2002, 54 sayfa

Bu tez, Casimir etkisinin hesaplanmasını sağlayacak bir algoritma kurulumunu ve sonrasında, bu algoritma vasıtasıyla etkinin uygulama alanlarını genişletip, laboratuvar koşullarında hazırlanması zor olan çeşitli geometrilerde bu etkiyi incelemeyi amaçlamaktadır. İlgili algoritmanın güvenilirliğini kontrol maksadı ile, hem deneysel, hem de teorik sonuçlar da verilmiş ve gözden geçirilmiştir.

Anahtar Kelimeler: Casimir Etkisi, Vakum Enerjisi, Atomsal Etkileşim Simülasyonu

ACKNOWLEDGEMENTS

I express my sincere gratefulness to Prof. Dr. Şakir Erkoç for his patience, guidance and tutorship. His directions and suggestions formed the guiding light for me in the field of simulations for which I had no prior experience. Also, he is the person that made it possible for me to investigate further in this topic and from a very different way. The adaptation process I had undergone in my first season in METU was overcome by the direct guidance and advices I took from him and other faculty members including but not limited to Prof. Dr. Sinan Bilikmen, Doç. Dr. Ayşe Karasu and department secretaries Sevim Aygar and Sultan Köksal. Without their help, it would be impossible for me to advance in such an enjoyment and eagerness. I also thank to Doç. Dr. Neşe Özdemir for attracting my attention to this subject at the first hand and being my tutor in my undergraduate thesis in ITU concerning another application of the subject. To my fiancée Bengü Yazıcıoğlu, I offer my deepest praises for her never ending faith in me. And for my mother, Dilek Kurtar, goes my kindest respects, with the expectation to having accomplished the task of being the son in her vision, so far.

PREFACE

"In recent years the method of "computer simulation" has started something like a revolution of science: the old division of physics (as well as chemistry, biology, etc.) into "experimental" and "theoretical" branches is no longer really complete. Rather, "computer simulation" has become a *third branch* complementary to the first two traditional approaches.

What, then, is the specific significance of computer simulation or "computer experiments"? The answer is simply that computer simulation yields *exact* information (apart from statistical errors, but these can be made as small as desired, at least in principle) on *model* systems which are precisely characterized. (For problems in statistical physics this means that parameters describing the Hamiltonian are known explicitly and exhaustively.)

In contrast, the information provided by analytic theory is exact only in rather rare cases, while in most other cases uncontrolled approximations are required. For example, statistical physics problems which are solvable for a three-dimensional geometry are idealized limiting cases such as ideal gases or

ideal solutions, coupled harmonic oscillators, etc. The statistical mechanics of even very simple models, such as the three-dimensional Ising model, cannot be solved exactly, and much less is known about models with realistic potentials between the atomic degrees of freedom. Thus computer simulations are often designed to check the accuracy of some approximation made in the analytical treatment of a model.

Similarly, the information provided by experiment is almost never precisely characterized in the sense that the effective Hamiltonian of a given experimental sample is precisely known. Sometimes it is even controversial whether some experimentally observed phenomenon is "intrinsic" or due to some unknown impurity effects – remember that the chemical constitution of an experimental sample is known only approximately anyway. These are just a few examples from which it is clear that the comparison between analytic theory and experiment does not always lead to conclusive answers, and simulations are needed to bridge this gap. Thus, a direct comparison between a simulation of a model and experiment is not hampered by inaccurate approximations, as are often inevitable in analytic theory, and hence may indicate more conclusively whether the model faithfully represents the real system or not."

K. Binder and D.W. Heermann[1]

TABLE OF CONTENTS

APPENDIX

LIST OF FIGURES

FIGURES

CHAPTER 1

INTRODUCTION

Starting from Casimir's 1948 dated article[2], the “Casimir-Polder”[3] reactions have been examined in various fields, some of which, aside from the quantum field theory, are cosmology and particle physics. Originally Casimir proposed the so called theory for the explanation of attraction between two parallel conducting plates. When two parallel conducting plates of unit area are placed in a vacuum at a distance from one another, they should be attracted by a force, which does not depend on mass, charge and any other coupling constants. The nature of this force may be considered as long-range, because of its dependency on the retardation [2]. Meanwhile, direct applications of these interactions are developed and the consequences of the effect have been verified through experiments including different types of conductors, as well

as semi-conductors and dielectrics. Since, unlike other interactions, the interaction energy and the sign of the arousing force in the Casimir effect depend vastly on the geometry of the system, our main interest in this work will be to investigate and gather some quantitative results for various geometries using simulation techniques, some of which, by practical means are very difficult to conduct using actual methods (mainly the atomic force microscopy) because of the closeness of the systems in question. Beginning with the basic geometries for which we have theoretical and experimental results, we will be able to confirm the appropriateness of our calculations and then, using these approved results, will continue to investigate the properties of more complex geometries such as concentric spherical shells, a spherical shell inside a cubic shell or a spherical shell confined within a pyramid.

In the second chapter, various methods that lead to the original Casimir results are explained. Using different approaches confirms the fact that, although the Casimir effect was firstly derived as a result of quantum electrodynamical phenomenon, it is not limited to this topic, as some relatively simple interactions also lead to the same result. By means of this identity, we will be able to calculate the effect using the summation of one-to-one atomic interactions. Milonni et al.'s book[4] and article[5], together with Mostepanenko et al.'s book[6] and article[7] and Elizalde and Romeo's article[8] were the main references for the derivations in this chapter. The

point splitting method, being one of the mostly used techniques for determining the Casimir energy was purposely omitted because of the complexity of the procedures involved when dealing with a relatively simple system: the process of calculating the Green functions required for each geometry and the space it is confined in would be overwhelming. Interested reader can find applications of this method in the works of Fulling[9], Birrell and Davies[10], and Bayın and Özcan[11].

In the third chapter, a brief review of some of the major experiments conducted so far is given with their results and their degrees of agreement with the theory.

Fourth chapter includes the algorithms and the results of our simulations, with graphical snap-shots.

Results and some possible after-developments are discussed in the last chapter where a synthesis of the three branches concerning the theory (the theory itself, the experiments and the simulations) is tried to be accomplished.

The proof of the analogy used in chapter 2 is included in the appendix section.

CHAPTER 2

THEORETICAL FOUNDATIONS OF THE CASIMIR EFFECT

2.1 Introduction

As a result of the vast application possibilities of the Casimir effect, various disciplines have been investigated and derived the effect using different techniques [4,6]. We have chosen derivations of the Casimir effect from the quantized electromagnetic field using electric and magnetic field operators, then with an another solution to the infinite summation by utilization of the Riemann - Zeta function and from a very different point of view, by calculating the momentum transferred from the virtual photons exerting pressure to the boundaries. Since each discipline has its own notation for various quantities, we tried to preserve these different notations as well.

2.2 The Casimir Effect derived from the Electromagnetic Interactions in the Vacuum State

In order to work with the appropriate operators, we must first define and quantize our field. This will allow us to acknowledge the vacuum state as the state where a defined annihilation operator has zero eigenvalue. Thus, we will first construct the field and define the necessary operators, and then will find the eigenvalues of the energy of the specific geometry defined by the boundary conditions in this field.

For a field with no boundaries, the number of allowed modes is infinite since there is no restriction on boundary conditions. With $\mathbf{A}(\mathbf{r})$ being the electromagnetic vector potential, from isotropy we conclude that $|A(r)|^2$ should be independent of $\mathbf{r}$ for each mode of the field. The Helmholtz equation

$$\nabla^2 \mathbf{A}_0(\mathbf{r}) + k^2 \mathbf{A}_0(\mathbf{r}) = 0, \qquad k = \frac{\omega}{c} \tag{1}$$

is satisfied by:

$$\mathbf{A}_0(\mathbf{r}) = e_{\mathbf{k}} e^{i\mathbf{k}\cdot\mathbf{r}}, \qquad \mathbf{k}\cdot\mathbf{e}_{\mathbf{k}} = 0 \tag{2}$$

so that

$$\nabla \mathbf{A}(\mathbf{r},t)=0 \tag{3}$$

which comes from the Coulomb Gauge.

If the space is divided into cubes of volume $V=L^3$ and with the periodic boundary condition we have

$$\mathbf{A}(x+L,y+L,z+L,t)=\mathbf{A}(x,y,z,t) \tag{4}$$

meaning

$$(k_x,k_y,k_z)=\frac{2\pi}{L}(n_x,n_y,n_z);\quad n_i \in \quad .$$

Further investigation of the vector potential yields[4]:

$$\mathbf{A}_{\mathbf{k}\lambda}\left(\mathbf{r},t\right)=\left(\frac{2\pi\hbar c^2}{\omega_k V}\right)^{\frac{1}{2}}\left[a_{\mathbf{k}\lambda}\left(t\right)e^{i\mathbf{k}\cdot\mathbf{r}}+a_{\mathbf{k}\lambda}^{\dagger}\left(t\right)e^{-i\mathbf{k}\cdot\mathbf{r}}\right]\mathbf{e}_{\mathbf{k}\lambda} \tag{10}$$

so

$$\mathbf{A}_{\mathbf{k}\lambda}\left(\mathbf{r},t\right)=\left(\frac{2\pi\hbar c^2}{\omega_k V}\right)^{\frac{1}{2}}\left[a_{\mathbf{k}\lambda}\left(0\right)e^{-i\left(\omega_k t-\mathbf{k}\cdot\mathbf{r}\right)}+a_{\mathbf{k}\lambda}^{\dagger}\left(t\right)e^{i\left(\omega_k t-\mathbf{k}\cdot\mathbf{r}\right)}\right]\mathbf{e}_{\mathbf{k}\lambda}. \tag{11}$$

From this point, the linearity of Maxwell's equations permits us to write the vector potential of the field as the sum of all possible modes:

$$\mathbf{A}\left(\mathbf{r},t\right)=\sum_{\mathbf{k}\lambda}\left(\frac{2\pi\hbar c^2}{\omega_k V}\right)^{\frac{1}{2}}\left[a_{\mathbf{k}\lambda}\left(t\right)e^{i\mathbf{k}\cdot\mathbf{r}}+a_{\mathbf{k}\lambda}^{\dagger}\left(t\right)e^{-i\mathbf{k}\cdot\mathbf{r}}\right]\mathbf{e}_{\mathbf{k}\lambda}. \tag{12}$$

From this vector potential, we derive the following electric and magnetic field operators[4]:

$$\mathbf{E}\left(\mathbf{r},t\right)=i\sum_{\mathbf{k}\lambda}\left(\frac{2\pi\hbar\omega_k}{V}\right)^{\frac{1}{2}}\left[a_{\mathbf{k}\lambda}\left(t\right)e^{i\mathbf{k}\cdot\mathbf{r}}+a_{\mathbf{k}\lambda}^{\dagger}\left(t\right)e^{-i\mathbf{k}\cdot\mathbf{r}}\right]\mathbf{e}_{\mathbf{k}\lambda}, \tag{13}$$

$$\mathbf{B}\left(\mathbf{r},t\right)=i\sum_{\mathbf{k}\lambda}\left(\frac{2\pi\hbar c^2}{\omega_k V}\right)^{\frac{1}{2}}\left[a_{\mathbf{k}\lambda}\left(t\right)e^{i\mathbf{k}\cdot\mathbf{r}}+a_{\mathbf{k}\lambda}\left(t\right)e^{-i\mathbf{k}\cdot\mathbf{r}}\right]\mathbf{k}\times\mathbf{e}_{\mathbf{k}\lambda}. \tag{14}$$

Now that we have the electromagnetic operators **A**, **E** and **B**, we can continue to construct the mode functions satisfying the boundary conditions and the quantization and normalization constraints valid through the geometry formed in the field.

For a setting of two semi-infinite parallel conducting plates placed at $z=0$ and $z=d$ respectively, with dimensions $L_x = L_y = L$ and L_z, the tangential component of the electric field must vanish on the plates. So, the normalized mode functions will be

$$\mathbf{A}(\mathbf{r}) = A_x(\mathbf{r})\mathbf{i} + A_y(\mathbf{r})\mathbf{j} + A_z(\mathbf{r})\mathbf{k} \tag{15}$$

where

$$A_x(\mathbf{r}) = \left(\frac{8}{V}\right)^{\frac{1}{2}} a_x \cos(k_x x)\sin(k_y y)\sin(k_z z) \tag{16}$$

$$A_y(\mathbf{r}) = \left(\frac{8}{V}\right)^{\frac{1}{2}} a_y \sin(k_x x)\cos(k_y y)\sin(k_z z) \tag{17}$$

$$A_z(\mathbf{r}) = \left(\frac{8}{V}\right)^{\frac{1}{2}} a_z \sin(k_x x)\sin(k_y y)\cos(k_z z) \tag{18}$$

with

$$\begin{aligned} &a_x^2 + a_y^2 + a_z^2 = 1, \qquad V = L^2 L_z, \\ &k_x = \frac{l\pi}{L},\ k_y = \frac{m\pi}{L},\ k_z = \frac{n\pi}{L_z}; \qquad l,m,n \in \mathbb{N}. \end{aligned} \tag{19}$$

Since $\nabla \cdot \mathbf{A} = 0$:

$$k_x A_x + k_y A_y + k_z A_z = \frac{\pi}{L}\left(lA_x + mA_y\right) + \frac{\pi}{L_z}\left(nA_z\right) = 0. \tag{20}$$

The allowed frequencies for these modes will simply be:

$$\omega_{lmn} = k_{lmn} c = \pi c \left[\frac{l^2}{L^2} + \frac{m^2}{L^2} + \frac{n^2}{L_z^2}\right]^{\frac{1}{2}}. \tag{21}$$

Thus, with an analogy to the harmonic oscillator [see Appendix A], the zero point energy of the vacuum inside the cavity will be:

$$\sum_{lmn}{}'(2)\left(\frac{1}{2}\hbar\omega_{lmn}\right)=\sum_{lmn}{}'\pi\hbar c\left[\frac{l^2}{L^2}+\frac{m^2}{L^2}+\frac{n^2}{L_z^2}\right]^{\frac{1}{2}} \tag{22}$$

The prime sign over the summation symbol indicate that a factor $\frac{1}{2}$ should be inserted if one of the integers l,m,n is zero – that is when we have only one polarization, in the other cases, the 2 factor arises from the two independent polarizations of modes with $l,m,n\neq 0$.

If $L\gg L_z=d$, then we can replace the summations over l and m with integrals with respect to $\mathrm{d}k_x$ and $\mathrm{d}k_y$:

$$\begin{aligned}E(d)&=\frac{L^2}{\pi^2}\hbar c\sum_n{}'\int_0^\infty \mathrm{d}k_x\int_0^\infty \mathrm{d}k_y\left(k_x^2+k_y^2+k_z^2\right)^{\frac{1}{2}}\\ E(d)&=\frac{L^2}{\pi^2}\hbar c\sum_n{}'\int_0^\infty \mathrm{d}k_x\int_0^\infty \mathrm{d}k_y\left(k_x^2+k_y^2+\frac{n^2\pi^2}{d^2}\right)^{\frac{1}{2}}\end{aligned} \tag{23}$$

which, is an infinite quantity. The zero-point energy of the vacuum is infinite even in a finite volume.

If the plates were taken apart from each other to an infinite, the sum over n in (23) could also be counted as an integral. This time:

$$E(\infty)=\frac{L^2}{\pi^2}\hbar c\frac{d}{\pi}\int_0^\infty \mathrm{d}k_x\int_0^\infty \mathrm{d}k_y\int_0^\infty \mathrm{d}k_z\left(k_x^2+k_y^2+k_z^2\right)^{\frac{1}{2}}. \tag{24}$$

These two energy functions are obviously infinite but, if we are to calculate the potential energy which is, by definition, the amount of energy required to construct the system – in other words, the energy that would take to move one of the plates from infinity to a vicinity of d with respect to the other one, we can calculate a finite value. This is done as follows:

$$U(d)=E(d)-E(\infty) \tag{25}$$

$$\begin{aligned}U(d)=\frac{L^2\hbar c}{\pi^2}\Bigg[&\sum_n{}'\int_0^\infty \mathrm{d}k_x\int_0^\infty \mathrm{d}k_y\left(k_x^2+k_y^2+\frac{n^2\pi^2}{d^2}\right)^{\frac{1}{2}}\\&-\frac{d}{\pi}\int_0^\infty \mathrm{d}k_x\int_0^\infty \mathrm{d}k_y\int_0^\infty \mathrm{d}k_z\left(k_x^2+k_y^2+k_z^2\right)^{\frac{1}{2}}\Bigg].\end{aligned} \tag{26}$$

If we refer to polar coordinates u,θ in the k_x,k_y plane $\left(\mathrm{d}k_x\mathrm{d}k_y=u\mathrm{d}u\mathrm{d}\theta\right)$

$$U(d)=\frac{L^2\hbar c}{\pi^2}\left(\frac{\pi}{2}\right)\left[\sum_n{}'\int_0^\infty \mathrm{d}u\,u\left(u^2+\frac{n^2\pi^2}{d^2}\right)^{\frac{1}{2}}-\frac{d}{\pi}\int_0^\infty \mathrm{d}k_z\int_0^\infty \mathrm{d}u\,u\left(u^2+k_z^2\right)^{\frac{1}{2}}\right]. \tag{27}$$

At this point, it is suitable to introduce a cut off function in the form of

$$f(k)=f\left(\left[u^2+k_z^2\right]^{\frac{1}{2}}\right) \tag{28}$$

such that

$$f(k)=\begin{cases}1; & k \ll k_m \\ 0; & k \gg k_m\end{cases}. \tag{29}$$

We might suppose $k_m \approx \frac{1}{a_0}$, where a_0 is the actual Bohr radius, because of the penetration of the wavelengths compared small with atomic dimensions. Now, equation (27) becomes

$$\begin{aligned} U(d) &= \frac{L^2\hbar c}{\pi^2}\left(\frac{\pi}{2}\right)\left[\sum_n{}'\int_0^\infty \mathrm{d}u\, u\left(u^2+\frac{n^2\pi^2}{d^2}\right)^{\frac{1}{2}} f\left(\left[u^2+k_z^2\right]^{\frac{1}{2}}\right)\right. \\ &\quad \left. -\frac{d}{\pi}\int_0^\infty \mathrm{d}k_z\int_0^\infty \mathrm{d}u\, u\left(u^2+k_z^2\right)^{\frac{1}{2}} f\left(\left[u^2+k_z^2\right]^{\frac{1}{2}}\right)\right] \\ &= \frac{L^2\hbar c}{4\pi}\left(\frac{\pi^3}{d^3}\right)\left[\sum_n{}'\int_0^\infty \mathrm{d}x\,\left(x+n^2\right)^{\frac{1}{2}} f\left(\frac{\pi}{d}\left[x+n^2\right]^{\frac{1}{2}}\right)\right. \\ &\quad \left. -\frac{d}{\pi}\int_0^\infty \mathrm{d}\kappa\int_0^\infty \mathrm{d}x\,\left(x+\kappa^2\right)^{\frac{1}{2}} f\left(\frac{\pi}{d}\left[x+\kappa^2\right]^{\frac{1}{2}}\right)\right]. \end{aligned} \tag{30}$$

where $x=\frac{u^2d^2}{\pi^2}$ and $\kappa=\frac{k_z d}{\pi}$.

Defining

$$F(\kappa)=\int_0^\infty \mathrm{d}x\left(x+\kappa^2\right)^{\frac{1}{2}} f\left(\frac{\pi}{d}\left[x+\kappa^2\right]^{\frac{1}{2}}\right) \tag{31}$$

$U(d)$ becomes

$$U(d)=\left(\frac{\pi^2\hbar c}{4d^3}\right)L^2\left[\frac{1}{2}F(0)+\sum_{n=1}^\infty F(n)-\int_0^\infty \mathrm{d}\kappa\, F(\kappa)\right]. \tag{32}$$

According to the Euler-MacLaurin summation formula[12]

$$\sum_{n=1}^\infty F(n)-\int_0^\infty \mathrm{d}\kappa\, F(\kappa)=-\frac{1}{2}F(0)-\frac{1}{12}F'(0)+\frac{1}{720}F'''(0)... \tag{33}$$

for $F(\infty)\to 0$. Using

$$\begin{aligned} F(\kappa) &= \int_{\kappa^2}^{\infty} \mathrm{d}u\,\sqrt{u}\,f\left(\frac{\pi}{d}\sqrt{u}\right), \\ F'(\kappa) &= -2\kappa^2 f\left(\frac{\pi}{d}\kappa\right) \end{aligned} \tag{34}$$

we have $F'(0)=0, F'''(0)=-4$ and all the higher derivatives $F^{(n)}(0)$ vanish if we assume that all the derivatives of the cut off function vanish at $\kappa=0$. Thus

$$\sum_{n=1}^{\infty} F(n) - \int_0^{\infty} \mathrm{d}\kappa\, F(\kappa) = -\frac{1}{2}F(0) - \frac{4}{720} \tag{35}$$

which makes

$$U(d) = \left(\frac{\pi^2\hbar c}{4d^3}\right)L^2\left(-\frac{4}{720}\right) = -\left(\frac{\pi^2\hbar c}{720d^3}\right)L^2. \tag{36}$$

Taking the derivative of this potential with respect to d, we acquire the attractive force per unit area between the plates:

$$F(d) = -\frac{\pi^2\hbar c}{240d^4} \tag{37}$$

which is just the result that Casimir had found in his original paper[2].

2.3 The Casimir Effect derived using the Zeta-Function

The application of the zeta-function regularization for calculating the Casimir effect in a perfectly conducting parallel-plate configuration can be

done as follows[8] (a more general application of this method concerning spheres and circles can be found in [13]):

The electromagnetic field in a three-dimensional space can be described as a composition of two scalar massless fields, one satisfying the Dirichlet boundary conditions and the other one satisfying the Neumann Boundary conditions. These fields correspond to the transverse electric and the transverse magnetic modes, and the conditions of the perfect conduction requires that $\mathbf{n}\bullet\mathbf{B} = 0$ and $\mathbf{n}\times\mathbf{E} = \mathbf{0}$ on the surface of the conductor, where $\mathbf{n}$ is the unit normal vector for the surface of the conductor. For these two modes, the eigenmodes have to satisfy the free Klein-Gordon equation

$$\Box\varphi(\mathbf{x},t) = 0. \tag{38}$$

The Dirichlet boundary conditions demand the field to (38) vanish on the boundaries:

$$\varphi^{D}(\mathbf{x},t) = 0. \tag{39}$$

If we assume the positions of the parallel-plates to be orthogonal to the x axis and separated by a distance L from each other, then, after renaming (x,y,z) into $\left(x,\mathbf{x_T}\right)$, the solutions may be expressed as

$$\begin{aligned}\varphi\left(x,\mathbf{x_T},t\right) &\sim \sin\left(\frac{\pi n x}{L}\right)e^{i\mathbf{k}_T\cdot\mathbf{x}_T}e^{-i\omega_{kn}^{D}(L)t}\\ \omega_{kn}^{D}(L) &= \left[\left(\frac{\pi n}{L}\right)^2+\mathbf{k}_T^2\right]^{\frac{1}{2}}, \qquad n = 1,2,3....\end{aligned} \tag{40}$$

And, for the eigenvalues obeying Neumann boundary conditions we have the constraint that

$$\partial_n \varphi^N(\mathbf{x},t)=0 \tag{41}$$

on the boundaries, n being the normal vector to the surface. Hence we get the eigenvalues obeying the Neumann boundary conditions as

$$\begin{aligned}\varphi\left(x,\mathbf{x}_{\mathbf{T}},t\right)&\sim\cos\left(\frac{\pi n x}{L}\right)e^{i\mathbf{k}_T\cdot\mathbf{x}_T}e^{-i\omega_{kn}^N(L)t}\\ \omega_{kn}^N(L)&=\left[\left(\frac{\pi n}{L}\right)^2+\mathbf{k}_T^2\right]^{\frac{1}{2}},\qquad n=0,1,2,3....\end{aligned} \tag{42}$$

Now we can write the field as a summation of these two sets of eigenvalues:

$$\begin{aligned}\varepsilon_0(L)&=\frac{1}{2}\left(\frac{1}{L}\sum_{n=1}^{\infty}\int\frac{\mathrm{d}^2\mathbf{k}_T}{(2\pi)^2}\omega_{kn}^D(L)+\frac{1}{L}\sum_{n=0}^{\infty}\int\frac{\mathrm{d}^2\mathbf{k}_T}{(2\pi)^2}\omega_{kn}^N(L)\right)\\&=\frac{1}{2L}\left(\sum_{n=1}^{\infty}+\sum_{n=0}^{\infty}\right)\int\frac{\mathrm{d}^2\mathbf{k}_T}{(2\pi)^2}\left[\left(\frac{\pi n}{L}\right)^2+\mathbf{k}_T^2\right]^{\frac{1}{2}}\\&=\frac{1}{2L}\int\frac{\mathrm{d}^2\mathbf{k}_T}{(2\pi)^2}\left(\mathbf{k}_T^2\right)^{\frac{1}{2}}+\frac{1}{L}\sum_{n=1}^{\infty}\int\frac{\mathrm{d}^2\mathbf{k}_T}{(2\pi)^2}\left[\left(\frac{\pi n}{L}\right)^2+\mathbf{k}_T^2\right]^{\frac{1}{2}}.\end{aligned} \tag{43}$$

To utilize the zeta-function, we replace the power $\frac{1}{2}$ by $-s/2$, where s is a complex variable:

$$\varepsilon_0(s,L)=\underbrace{\frac{1}{2L}\int\frac{\mathrm{d}^2\mathbf{k}_T}{(2\pi)^2}\left(\mathbf{k}_T^2\right)^{-s/2}}_{\varepsilon_0^{(1)}}+\underbrace{\frac{1}{L}\sum_{n=1}^{\infty}\int\frac{\mathrm{d}^2\mathbf{k}_T}{(2\pi)^2}\left[\left(\frac{\pi n}{L}\right)^2+\mathbf{k}_T^2\right]^{-s/2}}_{\varepsilon_0^{(2)}} \tag{44}$$

We will focus on $\varepsilon_0^{(2)}$ (the reason for this is the cancellation of the $\varepsilon_0^{(1)}$, as explained below). After assuming $\mathrm{Re}\,s$ to be large enough – one has to do this ansatz to make the integral result converging - we have [8]

$$\varepsilon_0^{(2)}(s,L)=\frac{\pi^{1-s}}{4L^{3-s}}\frac{\Gamma\left[(s-2)/2\right]}{\Gamma(s/2)}\sum_{n=1}^{\infty}\left(n^2\right)^{(2-s)/2}. \tag{45}$$

From the assumption that s was sufficiently large, the summation in (45) is actually the *Riemann zeta function* [12,13]

$$\zeta(z)=\sum_{n=1}^{\infty}n^{-z}, \qquad \mathrm{Re}\,z>1. \tag{46}$$

In this case, $\varepsilon_0^{(2)}$ would happen to be

$$\begin{aligned}\varepsilon_0^{(2)}(L)&=\lim_{s\to -1}\varepsilon_0^{(2)}(s,L)\\&=-\left(\frac{\pi^{\frac{3}{2}}}{8L^4}\right)\Gamma\left(-\tfrac{3}{2}\right)\zeta(-3).\end{aligned} \tag{47}$$

Since $\mathrm{Re}(-3)<1$, $\zeta(-3)$ can not be found from (46), but there are alternate methods to do this. On of these methods is the exploitation of the zeta function being multiplied by the gamma function, that is:

$$\Gamma\left(z/2\right)\zeta(z)=\pi^{z-1/2}\Gamma\left[(1-z)/2\right]\zeta(1-z) \tag{48}$$

so (47) reads:

$$\begin{aligned}\varepsilon_0^{(2)}(L)&=-\left(\frac{1}{8\pi^2L^4}\right)\zeta(4)\\&=-\frac{\pi^2}{720L^4}.\end{aligned} \tag{49}$$

As for $\varepsilon_0^{(1)}$, since we are looking for the difference of the energies at L and as $L\to\infty$, the ω_{kn} independent $\varepsilon_0^{(1)}$ term will yield the same results and hence, will cancel itself in the subtraction. $\varepsilon_0^{(2)}(L)$ will vanish for $L\to\infty$ because its dependency to L being $\sim 1/L^4$. So, at the end of the subtraction, we finally get

$$\varepsilon_0(L) = -\frac{\pi^2}{720L^4}. \tag{50}$$

Let $E(L)$ be the energy stored in the volume and $F(L)$ the Casimir force per area. Then (with the force being also in natural units, namely $\hbar = 1, c = 1$)

$$F(L) = \left(-\frac{\partial}{\partial L}\right)\overbrace{\left[L\varepsilon(L)\right]}^{E(L)} = -\frac{\pi^2}{240L^4}. \tag{51}$$

And thus, we have once more derived the original result that Casimir had found in his paper[2].

2.4 The Casimir Effect derived from the Momentum Transfer

In this approach, we focus ourselves on the linear momenta transferred by the virtual photons[4]. Each photon carries a momentum of $\frac{1}{2}\hbar\mathbf{k}$, and while the reflections outside the plates tend to push the plates together, the reflections inside the plates act to push the plates apart. Since, because of the frequency restrictions, the allowed fields outside of the plates are more than the ones inside, the net result of these reflections will be to push the plates together.

The pressure exerted by a plane wave with an angle of coincidence θ is

$$P = \frac{F}{A} = 2u\cos^2\theta \tag{52}$$

where u is the energy per unit volume of the incident field. Within the plates, a mode of frequency ω contributes a pressure

$$P = 2\left(\frac{1}{2}\right)\left(\frac{1}{2}\hbar\omega\right)V^{-1}\cos^2\theta = \frac{\hbar\omega}{2V}\frac{k_z^2}{k^2} \tag{53}$$

where $k = \frac{\omega}{c}$ and V is the quantization volume. The factor $\frac{1}{2}$ is needed in order to take the equally divided zero-point energies of the modes between the waves propagating towards or away from each of the plates into account[5]. For large plates, k_x and k_y take a continuum of values while k_z is discreet with $k_z = \frac{n\pi}{d}$ $(n \in \mathbb{N})$. Adding the contributions from all modes of the space between the plates, we have the total outward pressure

$$P_{out} = \frac{\hbar c}{\pi^2 d}\sum_{n=1}^{\infty}\int_0^{\infty} dk_x \int_0^{\infty} dk_y \frac{\left(n\pi/d\right)^2}{\left[k_x^2 + k_x^2 + \left(n\pi/d\right)^2\right]^{1/2}} \tag{54}$$

on each plate.

For the modes out of the plates, we simply let k_z to be continuous, therefore replacing $\sum_n$ with $\left(\frac{d}{\pi}\right)\int_0^{\infty} dk_z$:

$$P_{in} = \frac{\hbar c}{\pi^3}\int_0^{\infty} dk_x \int_0^{\infty} dk_y \int_0^{\infty} dk_z \frac{k_z^2}{\left[k_x^2 + k_x^2 + k_x^2\right]^{1/2}}. \tag{55}$$

Both P_{in} and P_{out} are infinite but, once more, we are interested in their difference. After some algebra (a similar approach is taken for (26)), we can write this difference as[4]:

$$P_{out} - P_{in} = \frac{\pi^2 \hbar c}{4d^4}\left[\sum_{n=1}^{\infty} \int_0^{\infty} \frac{dx}{\left(x + n^2\right)^{1/2}} - \int_0^{\infty} du\, u^2 \int_0^{\infty} \frac{dx}{\left(x + u^2\right)^{1/2}}\right] \tag{56}$$

and using the Euler-MacLaurin summation formula (33), we derive the force per unit area as

$$P_{out} - P_{in} = -\frac{\pi^2 \hbar c}{240 d^4} \tag{57}$$

just as the results found in the previous sections.

CHAPTER 3

THE EXPERIMENTAL VERIFICATIONS OF THE CASIMIR EFFECT

3.1 History

The Casimir force between two parallel metal plates was first measured by the experiment Spaarnay conducted in 1958[14]. Earlier and some of the experiments conducted after, used dielectrics as the media because of the interferometric methods allowed in order to determine the separation of the bodies. These experiments include the ones conducted by Derjaguin and Abrikosova[15], Derjaguin[16], Tabor and Winterton[17], Sabisky and Anderson[18]. Most of these experiments were able to confirm the predictions of the theory that, a critical change in the magnitude would happen for some critical separation but, they lacked the quantitative results because of the high

percentage error they included arising from the difficulty of keeping the two bodies parallel for such small separations and the actual smallness of the force. Although an abstract review of these major pioneering experiments will be given in section 3.3, two of the experiments conducted have importance for being the first in different aspects.

Abrikosova and Derjaguin used different configurations for the first time: a hemisphere over a flat surface of polished quartz, two flat plates of quartz, and one plate of quartz over a metal plate. The separation between them was measured by means of optical interferometry. They studied the force for the separations ranging from $0.1\mu\mathrm{m}$ to $0.4\mu\mathrm{m}$. Spaarnay's experiment was the first one to include conducting surfaces. The force between cleaned metal plates (chromium and aluminum) inside an evacuated chamber filled with nitrogen gas was measured by the restoring force on a spring to keep the system in balance. A great care was taken to keep the dust particles away, since they gave rise to repulsive forces. For separations between $0.5\mu\mathrm{m}$ and $2\mu\mathrm{m}$, forces between 0.2 dyne/cm^2 and 0.003 dyne/cm^2 were measured.

3.2 The Method

In most of the experiments, a spring, whose elastic modulus was known precisely, and a capacitor attached to the bodies were used in order to measure the restoring force and the separation distance accordingly.

As the two bodies attracted each other, the spring would resist the attraction and from a simple calculation, the force needed to restore the balance would be found. Also, the movement of one body with respect to other would change the separation distance between the plate of the capacitor attached to the moving body and the other plate attached to the stationary body resulting in the changing capacitance which can also be measured very precisely.

But, in Mohideen and Roy's experiment, a very modern method was used: they benefited from the accurate atomic force microscope (AFM) to measure the force between the two bodies. In their setup, a laser beam is reflected from the cantilever of the AFM holding up the sphere, and is received by a set of photodiodes. A force on the sphere would cause a deflection of the laser off the cantilever and there would be a signal difference among the photodiodes. By this means, they were able to collect data for separation differences ranging between 100 nm to 900 nm and so far, their

results are the most accurate results obtained, in excellent agreement with the theory.

3.3 The Experiments

3.3.1 Tabor and Winterton's Experiment (1968) [17]

Tabor and Winterton used extremely smooth mica cylinders having separations in units of Å. They measured the force between the sheets with their separations ranging from 50Å to 300Å. Their representation of the mica cylinders along with the results of their experiment taken from their original article are given in figure 1 and figure 2, respectively. The power change in the force resulting from the transition from the van der Waals interaction to the Casimir interaction can be clearly seen.

Figure 1: Tabor and Winterton's mica cylinders

Figure 2: Tabor and Winterton's results

3.3.2 Sabisky and Anderson's Experiment (1973) [18]

Helium films were utilized in this experiment where measurements for separations between 10Å and 250Å were achieved in very low temperature (1.38°K). They did not refer to Casimir's article, since their work consisted dielectrics, not conductors but, since their results were in excellent agreement with Lifshitz's theory[19] which also covered the same topic, their experiment was welcomed in favor of the Casimir effect. Although Lifshitz's theory's dealing with temperature was later corrected by the works of Mehra[20] and Brown and Maclay[21], this correction has negligible effect on Sabisky and

Anderson's experiment because of the low temperature involved. The scheme of their experiment is presented in figure 3 with their results for various measurements and calculations of the energy for different compounds in figure 4.

Figure 3: Sabisky and Anderson's vacuum can

Figure 4: Sabisky and Anderson's results

3.3.3 Sukenik et al.'s Experiment (1993) [22]

Contrary to the experiments done before, Sukenik measured the effect between a plate and atom. By means of passing sodium atoms in a gold cavity, he observed the deflection of the atoms from their usual route using the density (opacity in his case of sodium atoms) with respect to the change in the cavity width. His arrangement is given in figure 5. The results, as shown in figure 6, are in excellent agreement with Casimir's formulation. The labels in figure 6 are as follows: (a) Theoretical QED interaction, (b) theoretical van der Waals interaction, (c) no interaction at all.

Figure 5: Sukenik et al.'s arrangement

Figure 6: Sukenik et al.'s results

3.3.4 Lamoreaux's Experiment (1997) [23]

Along with Mohideen and Roy's experiment, Lamoreax's experiment is one of the most benefited experiment in theoretical studies. He measured the force originating from the Casimir effect for a system consisting of a 4 cm diameter sphere over a quartz plane with 0.5 cm thickness. He ran the

experiment for a separation range of 5000Å to 100000Å. His experimental arrangement along with his results are given in figure 7 and in figure 8, respectively.

Upper result graph shows data points against theoretical Casimir force with electric force subtracted and averaged, while lower graph shows theoretical Casimir force subtracted from the upper plot.

Figure 7: Lamoreaux's arrangement

Figure 8: Lamoreaux's results

3.3.5 Mohideen and Roy's Experiment (1998) [24]

As mentioned above, Mohideen and Roy's experiment is also, one of the basic experiments used for the verification of recent theories on the subject. This experiment has definite superiority over the ones preceding, including Lamoreaux's experiment. A totally new technology in measuring has been introduced in this experiment, that is, the utilization of the atomic force microscope (AFM) which enabled high accuracy in the measuring of the force for the smallest systems in question. They measured the force between a metallized (coated with 300 nm Al), $200 \pm 4\,\mu\mathrm{m}$ diameter sphere levitated above a sapphire disc. By means of the AFM, they were able to measure the

force for separations between 100 nm to 900 nm. The schematic arrangement of their experiment is given in figure 9, while an scanning tunneling microscope image is included in figure 10 with the results of their experiments being in figure 11.

Figure 9: Mohideen and Roy's arrangement

Figure 10: Mohideen and Roy's arrangment's STM image

Figure 11: Mohideen and Roy's results

CHAPTER 4

THE SIMULATIONS OF THE CASIMIR EFFECT

4.1 Introduction

In our simulation, we have calculated the overall energy stored in the systems via adding up and renormalizing the interatomic interaction energies. We will assume that the effect is additive and will show that, the total error for this assumption can not exceed 19.3% even for non-trivial geometries (reasons for the exactness of this factor will be explained below). The refining and renormalization processes are also explained. In our calculations, the FORTRAN-77 and PHP/C++ languages are used for compiling and running the code. The original code is developed by Şakir Erkoç[25] and it is modified for the Casimir theory. The results are then visualized through the 3-D

graphical engine controlled by Mathsoft Mathcad and finally, the graphs are plotted through the utilization of Microsoft Excel.

4.2 The Results of the "Additivity Assumption"

Casimir had found his results for two flat, parallel surfaces because of the simplicity of that arrangement offered for the calculations. In the experiments, as a result of the difficulty of aligning two flat surfaces parallel, a sphere over a plane is used most generally due to its symmetry and the ability to measure the difference between the two surfaces via the Newton rings formed on the plane. Since, the two parallel plate formation is the simplest geometry, a modification is needed when we are to investigate the effect in other geometries.

For such demands, Derjaguin developed a method[15] that relates the force between a sphere and a plane to the theoretically simpler two parallel flat planes, also known as the proximity force theorem[26]. The force between two spheres is given by[15]

$$F(d) \cong 2\pi \left(\frac{R_1 R_2}{R_1 + R_2} \right) u(d), \tag{58}$$

where $u(d)$ is the interaction energy per unit area between two flat surfaces separated by d, R_1 and R_2 being the radii of the spheres. For a sphere over a plane, we set the radius of one sphere to infinity and find

$$F(d) = 2\pi R u(d). \tag{59}$$

The theoretical Casimir potential for two perfectly conducting spheres is[27,28]

$$\varepsilon_S(d) = -\frac{143}{16\pi}\frac{R_1^3 R_2^3}{d^7} \tag{60}$$

where *d* is the distance between the spheres and R_k being the spheres' radii.

In our simulation, we derived the resultant energy from the atom-atom interactions. The formula for the Casimir potential between two atoms, with static electric and magnetic polarizabilities $\alpha_{E_k}(0)$, $\alpha_{M_k}(0)$ and separated by a distance r is given by[2]:

$$U(r) = \frac{C}{r^7} \tag{61}$$

where

$$C = -\frac{23}{4\pi}\left(\alpha_{E_1}\alpha_{E_2} + \alpha_{M_1}\alpha_{M_2}\right) + \frac{7}{4\pi}\left(\alpha_{E_1}\alpha_{M_2} + \alpha_{E_2}\alpha_{M_1}\right). \tag{62}$$

After calculating this potential via summing up the one-to-one interactions (61) for the two spheres, we have:

$$U_S^A(d) = \frac{16}{9}\pi^2 C N_1 N_2 R_1^3 R_2^3 / d^7 \tag{63}$$

$N_{1,2}$ being the atomic number densities in the spheres. Since the geometry with the most accurate calculation (i.e., the one that hasn't been subject to any approximations) for the Casimir effect is the case of two flat, parallel plates (geometrically, two half-spaces compared to atomic penetration depth), we will be using this system as a reference to the other systems. The interaction potential energy calculated using (61) for two flat, parallel planes is[7]

$$U_P^A(d) = -\frac{C N_1 N_2}{\pi/24}\varepsilon_P(d) \tag{64}$$

where

$$\varepsilon_P(d) = -\frac{\pi^2}{720}\frac{1}{d^3} \tag{65}$$

and the superscript A over U representing that the result is found using the additivity principle. Using the well-known formula for the Casimir potential of two half-spaces separated by a distance *d*:

$$U_P(d) = -\frac{\pi^2}{720 d^3} \tag{66}$$

we can now define the renormalization factor U_P^A / U_P as:

$$U_P^A / U_P = \frac{C N_1 N_2}{\pi/24} \tag{67}$$

dividing $U_S^A(d)$ with (67), we finally find the renormalized potential for two spheres:

$$\varepsilon_S^A(d) = -\frac{2\pi^3}{27}\frac{R_1^3 R_2^3}{d^7}. \tag{68}$$

The comparison of (68) with the formerly known theoretical result (60) yields that even for the case of two spheres being the maximally deviating geometry with respect to the two half-planes, the error arising from the assumption of the additivity principle can not exceed 19.3%; this error only depends on the geometry of the system – not to the separation distance. Since, we will focus on the relative differences of various systems, this error is acceptable.

An alternative calculation method is proposed in Hult et al.'s paper[29].

4.3 The Formation of the Geometries

To form the geometries needed, we first filled an empty 3-dimensional space, with spheres whose radii and separations were based on the fcc structured aluminum atoms. Then, with the help of selection algorithms, we have chosen the suitable atoms in order to form the geometries in question. Examples of these algorithms are as follows (PHP code):

```
for($counter=0; $counter<$satirsayisi; $counter++)
{
      $n = sscanf($mesaj[$counter], "%f %f %f %d"
            , &$atomx, &$atomy, &$atomz, &$atomno);
      if($n != 4) echo "\n<b>hatali satir $counter </b>\n";

      $bos1= 12-strlen("$atomx");
      $bos2= 12-strlen("$atomy");
      $bos3= 12-strlen("$atomz");
      $bos4=12-strlen("$atomno");
      $satir=str_repeat(" ",$bos1).$atomx
            .str_repeat(" ",$bos2).$atomy
            .str_repeat(" ",$bos3).$atomz
            .str_repeat(" ",$bos4).$atomno."\n";

      if(
           (abs($atomx)>=$mins&&abs($atomx)<=$maks)
         ||(abs($atomy)>=$mins&&abs($atomy)<=$maks)
         ||(abs($atomz)>=$mins&&abs($atomz)<=$maks)
        ){echo $satir;fwrite($fp,"$satir");}
}
```

In this code, '$mesaj[$counter]' is passed as a string in the form:

```
36.44991    32.39992   -12.14997     24768
```

where the first three numbers are the atom's coordinates in the x, y, z-axes accordingly and the fourth is the atom label. The file including all of the atoms' positions is generated by Şakir Erkoç's program. The code parses these numbers as the '$atomx', '$atomy', '$atomz' and '$atomno' variables and formats these data in a standard form with the help of the 'str_len' and the 'str_repeat' command. Then it checks if the coordinates fulfill the requirements imposed by the boundary conditions, namely '$mins' and '$maks', denoting the interval for an axis.

Similarly, the algorithm for generating a sphere having a shell between the two radii ‘$rmin’ and ‘$rmaks’ is handled by the following code:

```
for($counter=0; $counter<$satirsayisi; $counter++)
{
      $n = sscanf($mesaj[$counter], "%f %f %f %d"
            , &$atomx, &$atomy, &$atomz, &$atomno);
      if($n != 4) echo "\n<b>hatali satir $counter </b>\n";
      $yaricap=sqrt(pow($atomx,2)+pow($atomy,2)+pow($atomz,2));
      $bos1= 12-strlen("$atomx");
      $bos2= 12-strlen("$atomy");
      $bos3= 12-strlen("$atomz");
      $bos4=12-strlen("$atomno");
      //$atomz+=10;
      $satir=str_repeat(" ",$bos1).$atomx
            .str_repeat(" ",$bos2).$atomy
            .str_repeat(" ",$bos3).$atomz
            .str_repeat(" ",$bos4).$atomno."\n";

      if($yaricap<=$rmaks                        &&$yaricap>=$rmin){echo
$satir;fwrite($fp,"$satir");}

}
```

and for a pyramid with a square having sides of length ‘$taban’ as base and with a height ‘$yuksek’, we manipulate the code as follows:

```
for($counter=0; $counter<$satirsayisi; $counter++)
{
      $n = sscanf($mesaj[$counter], "%f %f %f %d"
                , &$atomx, &$atomy, &$atomz, &$atomno);
      if($n != 4) echo "\n<b>hatali satir $counter </b>\n";

      $bos1= 12-strlen("$atomx");
      $bos2= 12-strlen("$atomy");
      $bos3= 12-strlen("$atomz");
      $bos4= 12-strlen("$atomno");
      $satir=str_repeat(" ",$bos1).$atomx
            .str_repeat(" ",$bos2).$atomy
            .str_repeat(" ",$bos3).$atomz
            .str_repeat(" ",$bos4).$atomno."\n";

      $aa=$taban*($yuksek-$atomz)/(2.0*$yuksek);
      $a = $aa / 2.0;
      if(abs($atomz)>0&&$atomz<=$yuksek)
      {
```

```
            if(abs(abs($atomx)-$a) < $eps && abs($atomy) >= 0
               && abs($atomy) <= $a)
               {echo $satir;fwrite($fp,"$satir");}
            if(abs(abs($atomy)-$a) < $eps && abs($atomx) >= 0
               && abs($atomx) <= $a)
               {echo $satir;fwrite($fp,"$satir");}
      }
      if($atomz<-35)
      {
            if(abs($atomy) >= 0 && abs($atomy) <= $a
               && abs($atomx) >= 0 && abs($atomx) <= $a)
               {echo "<b>$satir</b>";fwrite($fp,"$satir");}
      }
}
```

4.4 The Algorithm used in the Simulation

Since the r^{-7} factor in the formulae yields to some large values when "very near atoms' interactions" occur, and also because of the fact that, at such small distances, the Casimir-Polder interactions are interferred grossly by the van der Waals interactions ($\sim r^{-6}$), these small-separation factors were eliminated from the calculations. This is achieved by a simple control algorithm checking the relative distances between the two atoms in question. The algorithm also prevented the calculation of the Casimir potential in between the atoms of the same surface. This second procedure was also required since, the energy difference between the energy of the isolated surfaces and the energy of the formed system is in importance, not their isolated values. The part of the code producing this algorithm is as follows (FORTRAN-77 code):

```
SLABSON=6400
IF(J.LT.I) GO TO 30
IF(I.LE.SLABSON.AND.J.LE.SLABSON) GO TO 30
IF(I.GT.SLABSON.AND.J.GT.SLABSON) GO TO 30
IF(J.EQ.I) GO TO 30
```

Here, there are three variables, namely the ‘I’, ‘J’ and ‘SLABSON’. ‘I’ and ‘J’ are the labels of the two atoms in question, while ‘SLABSON’ gives the total number of atoms in one body. The control algorithm first checks if ‘J’ is lower than ‘I’, so that, only the atoms that have greater atom number are considered, thus preventing the recalculation of the interaction between the same atoms more than once. Then, it checks if the first and the second atoms belong to the first body or, in the next sentence if they are both on the second body: if they are, than there is no need to calculate, since, we’re interested only in the interaction between the atoms on different bodies. Lastly, the algorithm checks if these two atoms are identical, thus preventing a loop-hole where the case is 0 units separation.

4.5 The Scaling Factor

After the calculations, it has been observed that, the elimination of very near atom interactions wasn't sufficient enough to achieve the experimental and the theoretical results: the relatively small simulation system was still coping with the calculations due to its relatively short inter-atomic distance.

To overcome this factor, we ran the simulation of a well known system (being the two parallel slabs) for numerous times and tried to achieve the converging value. The graph of these runs can be seen in Figure 12.

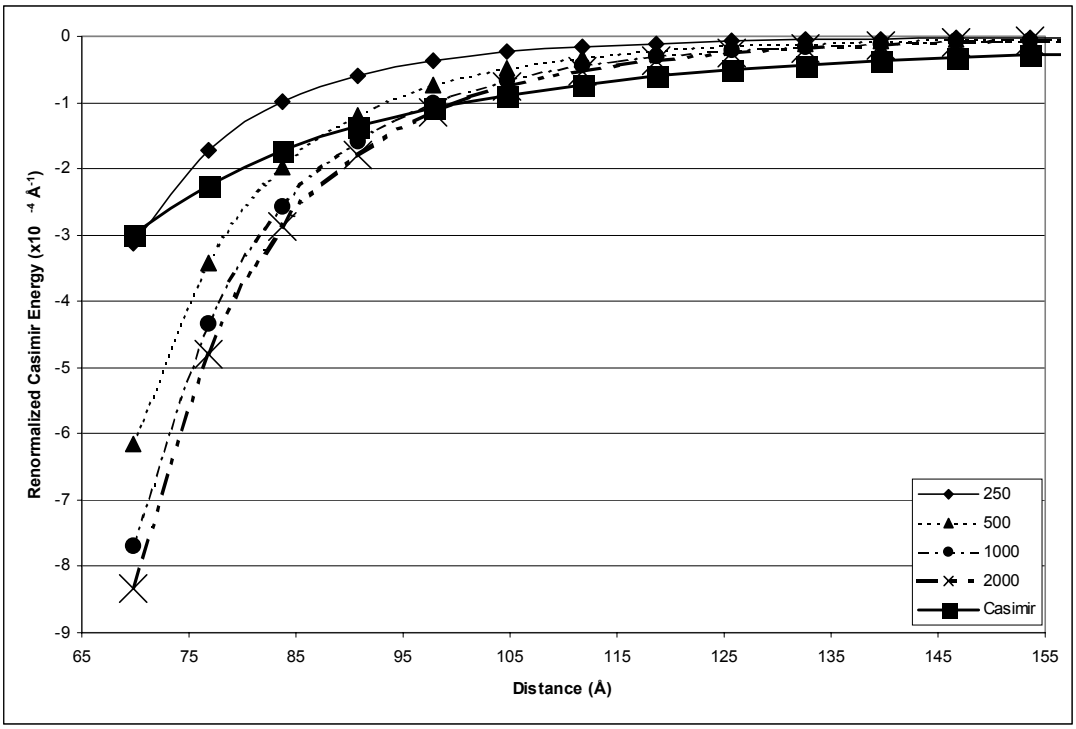

Figure 12: Renormalized energy graph vs. distance for paralel slab formation. The legend shows the number of atoms in each slab. The solid line represents the theoretical Casimir energy.

In this graph, Casimir potentials of slabs consisting of different number of atoms are plotted with the theoretical Casimir potentials corresponding to the appropriate distances. The distances are in Å, while, the energies are in $\frac{1}{\text{Å}}$ where natural unit system is used ($\hbar = 1, c = 1$).

Similar processes are done with other trivial systems such as "Atom vs. Atom" and "Atom vs. Slab" and as expected, it has been seen that, these runs also yielded similar convergences. "Atom vs. Slab" system results can be seen in Figure 13.

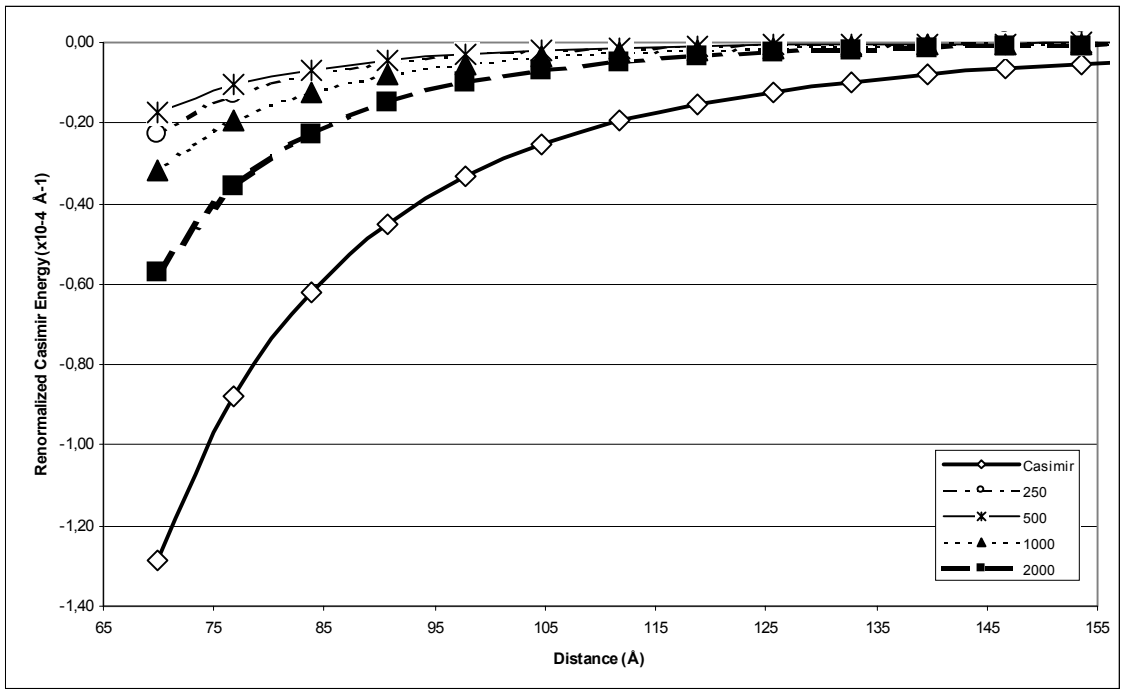

Figure 13: Renormalized energy graph vs. distance for atom vs. slab formation. The legend shows the number of atoms in the slab. The solid line represents the theoretical Casimir energy.

In this graph, Casimir potentials of slabs consisting of different number of atoms within vicinity of a single atom are plotted with the theoretical Casimir potentials corresponding to the appropriate distances. The distances are in Å, while, the energies are in $\frac{1}{\text{Å}}$ where natural unit system is used ($\hbar = 1, c = 1$).

Using the approximate ratios between the appropriate system's converging energy factor and the theoretical Casimir potential, the scaling factor is obtained. This rationing method is based primarily on the method used for renormalizing the non-trivial topology-caused deflections which is derived by Mostepanenko and Trunov that is explained in section 4.2. But, since the geometries include contained systems, the error will, in general, be higher than the original renormalization method's error.

4.6 The Results

By means of the techniques explained above, we were able to calculate the Casimir potentials for the following geometries:

4.6.1. Concentric Spherical Shells

In this model, the inner shell with radius 7 to 10 Å contains 170 atoms and the outer shell with radius 37 to 40 Å contains 3336 atoms as shown in figure 14. The renormalized energy for this model is calculated as $-7.2411261 \times 10^{-4}$ Å^{-1} (in natural units).

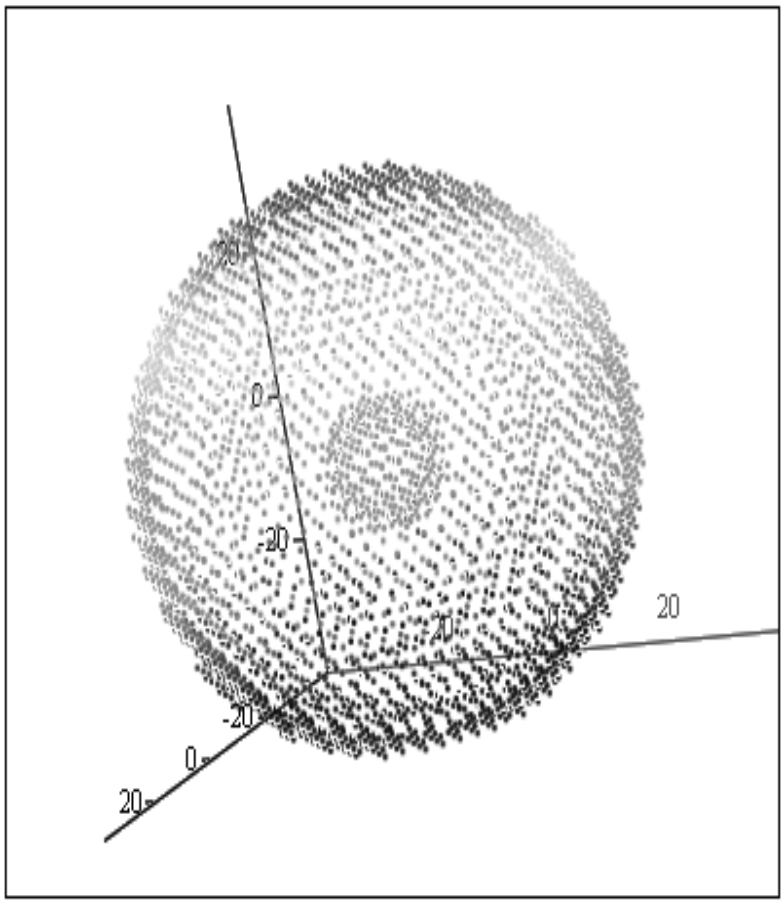

Figure 14: Concentric spherical shells

4.6.2. A Spherical Shell Inside A Cubic Shell

In this model, the spherical shell with radius 30 to 34 Å contains 3090 atoms and the cubic shell with line lengths 35 to 40 Å contains 5999 atoms as shown in figure 15. The renormalized energy for this model is calculated as $-5.449791\,\text{Å}^{-1}$ (in natural units).

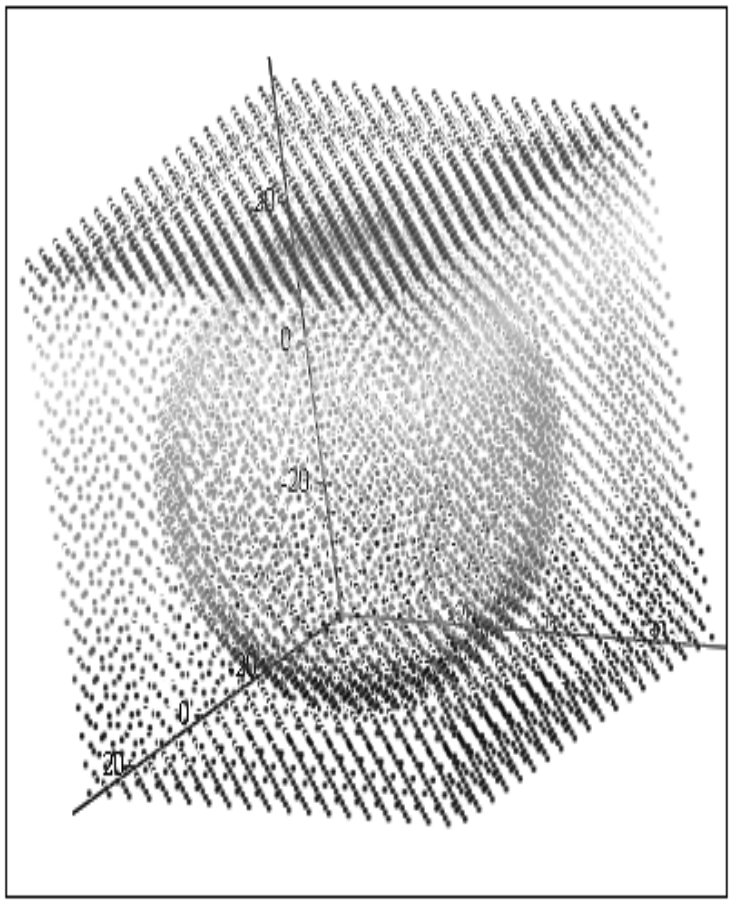

Figure 15: Spherical shell inside a cubic shell

4.6.3. A Spherical Shell Inside A Pyramid

In this model, the spherical shell with radius 7 to 10 Å contains 170 atoms and the pyramid with dimensions 20x20x35 Å contains 1057 atoms as shown in figure 16. The renormalized energy for this model is calculated as $-1.426447\,\text{Å}^{-1}$ (in natural units).

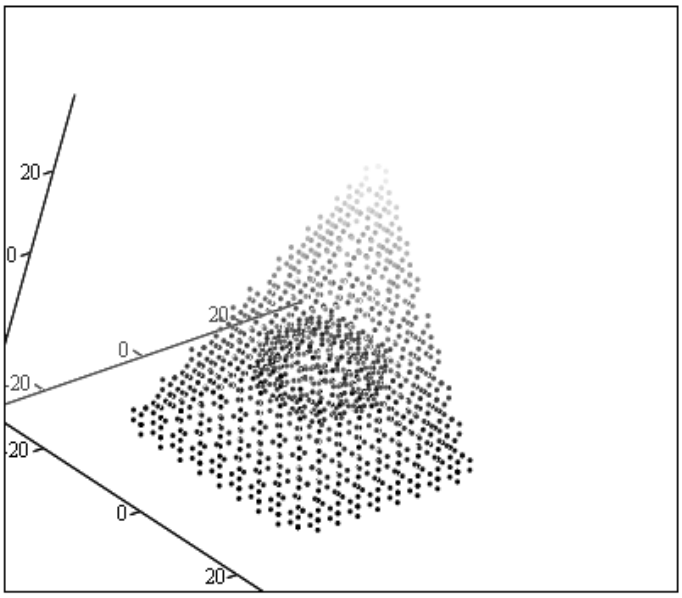

Figure 16: Spherical shell inside a pyramid

4.7 Discussion and Conclusions

As can be verified from the results above, using relatively small systems in the simulation results in high potentials. But, since we are interested in the comparisons of these geometries, this is acceptable. We see that, when parallel surfaces are used, the energy stored in the system is relatively small when compared with a system consisting two different geometries. The systems formed by different types of geometries can be used for storing energy because of the sign dependence of the Casimir force on the geometry. In a recent article written by Manzoni and Wreszinski[30], the repulsive force in the case of a cube, sliced from the half was calculated. A similar calculation was done many years ago by Boyer[31] concerning a sphere sliced from the half. Were the experiments of these theoretical situations done with the concentric systems included, our predictions based on the simulation shows that, a considerable, measurable force sign change would occur. However, we don't expect the experimental measurement of these systems to happen in a near future because of the difficulties in forming such small, properly oriented systems and the current measurement techniques' lacking of proper measuring the force from inside the container shell without interfering with the system itself. As we tried to explain above, both the old techniques (including the capacitor - spring combination) and the new techniques (including the atomic force microscope which measures the

deflection of the incident laser from the surface) are incapable of coping with the systems simulated. We have used aluminum atoms for them being mostly used in experiments.

In our simulations, we didn't take account of the temperature and the surface roughness of the system, but this can also be accepted since, in simulation, all of the systems were assumed to be in the same condition, thus, making our comparisons more reliable. Details of refining with respect to temperature and surface roughness can be found in experimental and guidance articles [6, 22 - 24, 32]. We have considered the systems for a single condition – variations in the conditions are easily applicable including various separation distances.

4 days prior to this thesis' presentation, an article written by Ahmedov and Duru was submitted to the *arxiv.org* e-text library giving a full theoretical solution to the concrete spherical shells formation [33]. Now that we have an exact solution for one of the systems considered in this thesis, more successfull algorithms can be derived and developed.

The simulation can be applied to more complex geometries like a triple concentric cubes, spheres or systems consisting of other systems as building

blocks like a cube constructed by two or more pyramids. Also, an interesting geometry would be a configuration of three parallel slabs.

REFERENCES

[1] Binder, K., Heermann, D.W., *Monte Carlo Simulation in Statistical Physics,* Springer-Verlag, Germany (1997).

[2] Casimir, H.B.G., *Proc. K. Ned. Akad. Wet*. **51**, 793 (1948).

[3] Casimir, H.B.G., Polder, D., Phys. Rev. **73**, 360 (1948).

[4] Milonni, P.W., *The Quantum Vacuum*, Academic Pres Inc, USA (1994).

[5] Milonni, P.W., Shih, M.L., *Contemp. Phys.,* **33**, 313 (1992).

[6] Mostepanenko, V.M., Trunov, N.N., *The Casimir Effect and Its Applications,* Clarendon, UK (1997).

[7] Bordag, M., Mohideen U., Mostepanenko V.M., *quant-ph/0106045* (2001).

[8] Elizalde, E., Romeo, A., *Am. J. Phys.,* **59**, 711 (1991).

[9] Fulling, S.A., *Aspects of Quantum Field Theory in Curved Space-Time*, Cambridge University Press, UK (1989).

[10] Birrell, N.D., Davies, P.C.W., *Quantum Fields in Curved Space*, Cambridge University Press, UK (1986).

[11] Bayın, S.Ş., Özcan, M., *Phys. Rev. D*, **49**, 5313 (1994).

[12] Mathews, J., Walker, R.L., *Mathematical Methods of Physics*, W.A. Benjamin Inc., USA (1965).

[13] Leseduarte, S., Romeo, A., *Ann. Phys.*, **250**, 448 (1996).

[14] Spaarnay, M.J., *Physica*, **24**, 751 (1958).

[15] Derjaguin, B.V., Abrikosova, I.I., *Sov. Phys. JETP* **3**, 819 (1957).

[16] Derjaguin, B.V., *Sci. Am.* **203**, 47 (1960).

[17] Tabor, D., Winterton, R.H.S., *Nature*, **219**, 1120 (1968).

[18] Sabisky, E.S., Anderson, C.H., *Phys. Rev. A*, **7**, 790 (1973).

[19] Lifshitz, E.M., *Sov. Phys. JETP,* **2**, 73 (1956).

[20] Mehra, J., *Physica,* **37**, 145 (1967).

[21] Brown, L.S., Maclay, G.J., *Phys. Rev.,* **184**, 1272 (1979).

[22] Sukenik, C.I., Boshier, M.G., Cho, D., Sandoghdar, V., Hinds, E.A., *Phys. Rev. Lett.,* **70**, 560 (1993).

[23] Lamoreaux, S.K., *Phys. Rev. Lett.,* **78**, 5, (1997). Erratum was published in: Lamoreaux, S.K., *Phys. Rev. Lett.,* **81**, 5475 (1998).

[24] Mohideen, U., Roy, A., *Phys. Rev. Lett.,* **81**, 4549 (1998).

[25] Erkoç, Ş., *Molecular-Dynamics Program For Cluster Simulations (Modified for the van der Waals interactions)*, 2000.

[26] Blocki, J., Randrup, J., Swiatecki, W.J., Tsang, C.F., *Ann. Phys.* **105**, 427 (1977).

[27] Feinberg, G., *Phys. Rev. B*, **9**, 2490 (1974).

[28] Ford, L.H., *Phys. Rev. A*, **25**, 135 (1982).

[29] Hult, E., Rydberg, H., Lundqvist, B.I., *cond-mat/9805352* (1998).

[30] Manzoni, L.A., Wreszinski, W.F., *Phys. Lett. A*, **292**, 156 (2001).

[31] Boyer, T.H., *Phys. Rev.*, **174**, 1764 (1969).

[32] Goedecke, G.H., Wood, R.C., *Phys. Rev. A*, **60**, 2577 (1999).

[33] Ahmedov, H., Duru, I.H., *hep-th/0207186v1* (2002).

APPENDIX

PROOF: A FIELD MODE IS IDENTICAL TO A HARMONIC OSCILLATOR[4,6]

The Maxwell equations for the "free" field (the field in a region where there are no sources are):

$$\nabla \cdot \mathbf{E} = 0 \tag{1}$$

$$\nabla \cdot \mathbf{B} = 0 \tag{2}$$

$$\nabla \times \mathbf{E} = -\frac{1}{c}\frac{\partial \mathbf{B}}{\partial t} \tag{3}$$

$$\nabla \times \mathbf{B} = \frac{1}{c}\frac{\partial \mathbf{E}}{\partial t} \tag{4}$$

$$\mathbf{B} = \nabla \times \mathbf{A} \tag{5}$$

Since $\nabla \cdot (\nabla \cdot \mathbf{A}) = 0$, (2) is also satisfied. (3) implies $\mathbf{E} = -\left(\frac{1}{c}\right)\frac{\partial \mathbf{A}}{\partial t} - \nabla\phi$, where ϕ is the scalar potential. From (4), we derive

$$\nabla^2 \mathbf{A} - \frac{1}{c^2}\frac{\partial^2 \mathbf{A}}{\partial t^2} = 0 \tag{6}$$

for the Coulomb gauge defined by $\nabla \cdot \mathbf{A} = 0$ and in the absence of any sources $(\phi = 0)$. Now, (1) is also satisfied. Therefore, we can obtain a solution of the free space Maxwell equations by solving (6) for the Coulomb gauge vector potential subject to the appropriate boundary conditions.

Separation of variables gives monochromatic solutions

$$\begin{aligned} \mathbf{A}(\mathbf{r},t) &= \alpha(t)\mathbf{A}_0(\mathbf{r}) + \alpha^*(t)\mathbf{A}_0^*(\mathbf{r}) \\ &= \alpha(0)e^{-i\omega t}\mathbf{A}_0(\mathbf{r}) + \alpha^*(t)e^{i\omega t}\mathbf{A}_0^*(\mathbf{r}) \end{aligned} \tag{7}$$

where $\mathbf{A}_0(\mathbf{r})$ satisfies the Helmholtz equation

$$\nabla^2 \mathbf{A}_0(\mathbf{r}) + k^2 \mathbf{A}_0(\mathbf{r}) = 0 \qquad (k = \omega / c) \tag{8}$$

and $\alpha(t)$ satisfies $\ddot{\alpha}(t) = -\omega^2 \alpha(t)$. Then, the electric and magnetic field vectors are given by

$$\begin{aligned} \mathbf{E}(\mathbf{r},t) &= -\frac{1}{c}\left[\dot{\alpha}(t)\mathbf{A}_0(\mathbf{r}) + \dot{\alpha}^*(t)\mathbf{A}_0^*(\mathbf{r})\right], \\ \mathbf{B}(\mathbf{r},t) &= \alpha(t)\nabla \times \mathbf{A}_0(\mathbf{r}) + \dot{\alpha}^*(t)\nabla \times \mathbf{A}_0^*(\mathbf{r}). \end{aligned} \tag{9}$$

The electromagnetic energy is proportional to

$$\begin{aligned} \int \mathrm{d}^3 r \left(\mathbf{E}^2 + \mathbf{B}^2\right) = {} & \frac{1}{c^2}\dot{\alpha}(t)^2 \int \mathrm{d}^3 r\, \mathbf{A}_0(\mathbf{r})^2 + \frac{1}{c^2}\dot{\alpha}^*(t) \int \mathrm{d}^3 r\, \mathbf{A}_0^*(\mathbf{r})^2 \\ & + \frac{2}{c^2}\left|\dot{\alpha}(t)\right| \int \mathrm{d}^3 r \left|\mathbf{A}_0(\mathbf{r})^2\right| + \alpha(t)^2 \int \mathrm{d}^3 r \left[\nabla \times \mathbf{A}_0(\mathbf{r})\right]^2 \\ & + \dot{\alpha}^*(t)^2 \int \mathrm{d}^3 r \left[\nabla \times \mathbf{A}_0^*(\mathbf{r})\right]^2 \\ & + 2\left|\dot{\alpha}(t)\right|^2 \int \mathrm{d}^3 r \left|\nabla \times \mathbf{A}_0(\mathbf{r})\right|^2 . \nabla \times \mathbf{A}_0^*(\mathbf{r}). \end{aligned} \tag{10}$$

If we take

$$\int \mathrm{d}^3 r \left[\nabla \times \mathbf{A}_0(\mathbf{r})\right]^2 = k^2 \int \mathrm{d}^3 r\, \mathbf{A}_0(\mathbf{r})^2 \tag{11}$$

and with similar expressions for the terms involving $\left[\nabla \times \mathbf{A}_0^*(\mathbf{r})\right]^2$ and $\left|\nabla \times \mathbf{A}_0(\mathbf{r})\right|^2$ in (10) with $\dot{\alpha}(t)^2 = -\omega^2 \alpha(t)^2$ since $\dot{\alpha}(t) = -i\omega\alpha(t)$, then (10) simplifies to

$$H_F = \frac{1}{8\pi} \int \mathrm{d}^3 r \left(\mathbf{E}^2 + \mathbf{B}^2\right) = \frac{k^2}{2\pi} \left|\alpha(t)\right|^2 \tag{12}$$

where we assumed the mode function $\mathbf{A}_0(\mathbf{r})$ is normalized

$$\left(\int \mathrm{d}^3 r \left|\mathbf{A}_0(\mathbf{r})\right|^2 = 1\right). \tag{13}$$

If we define the real quantities

$$q(t) = \frac{i}{c\sqrt{4\pi}} \left[\alpha(t) - \alpha^*(t)\right], \tag{14}$$

$$p(t) = \frac{k}{\sqrt{4\pi}} \left[\alpha(t) + \alpha^*(t)\right] \tag{15}$$

equation (12) becomes

$$H_F = \frac{1}{2}\left(p^2 + \omega^2 q^2\right). \tag{16}$$

This means that, our field mode of frequency ω is mathematically equivalent to a harmonic oscillator with frequency ω.